

UKAEA-CCFE-PR(18)59

Marco Cecconello, A. Sperduti

The Neutron Camera Upgrade for MAST Upgrade

Enquiries about copyright and reproduction should in the first instance be addressed to the
UKAEA

Publications Officer, Culham Science Centre, Building K1/O/83 Abingdon, Oxfordshire,
OX14 3DB, UK. The United Kingdom Atomic Energy Authority is the copyright holder.

The Neutron Camera Upgrade for MAST Upgrade

Marco Cecconello, A. Sperduti

The Neutron Camera Upgrade for MAST Upgrade^{a)}

M. Cecconello,^{1, b)} A. Sperduti,¹ I. Fitzgerald,² S. Conroy,¹ S. J. Holm,¹ and M. Weiszflog¹

¹⁾*Department of Physics and Astronomy, Uppsala University, EURATOM-VR Association, Uppsala, Sweden*

²⁾*EURATOM/CCFE Fusion Association, Culham Science Centre, Abingdon, United Kingdom*

(Dated: 10 June 2018)

The Neutron Camera Upgrade (NCU) is a neutron flux monitor consisting of six lines of sight under installation on MAST Upgrade. The NCU is expected to contribute to the study of the confinement of fast ions and on the efficiency of non-inductive current drive in presence of on-axis and off-axis neutral beam injection by measuring the neutron emissivity profile along the equatorial plane. This paper discusses the NCU main design criteria, the engineering and interfacing issues and the solutions adopted. In addition, results from the characterization and performance studies of the neutron detectors using standard γ -rays sources and a ^{252}Cf source are discussed. The proposed design has a time resolution of 1 ms with a statistical uncertainty of less than 10 % for all MAST Upgrade scenarios with a spatial resolution of 10 cm: higher spatial resolution is possible by moving the lines of sight in-between plasma discharges. The energy resolution of the neutron detector is better than 10 % for a light output of 0.8 MeVee and the measured pulse shape discrimination is satisfactory.

Keywords: MAST Upgrade, neutron camera, liquid scintillator, pulse shape discrimination, energy resolution function

I. INTRODUCTION

A crucial aspect for future fusion power plants is the maximization of fusion power production which depends also on the confinement of fast ions and in particular of α -particles from DT reactions. In preparation for ITER operation, fast ions physics studies are carried out in present-day fusion devices where MHD instabilities similar to those expected to be driven by α -particles can be observed.

In particular, Spherical Tokamaks (STs) are well suited to contribute to the study and understanding of fast ion physics in ITER-relevant regimes. This is made possible by the combination of a low confining magnetic field and Neutral Beam Injection (NBI) resulting in a super-Alfvénic fast ion population which, in turn, can excite a whole range of energetic particle modes. Measurements of the confined fast ion population can either be done directly, for example by using fast ion D_α spectrometry (FIDA), or, indirectly, by using fusion product detectors. This is possible thanks to the fact that, in present-day NBI heated STs, almost all the fusion products emission is strongly dependent on and dominated by the beam-thermal component (≈ 90 % of the total emission).

On the Mega Ampere Spherical Tokamak¹ (MAST), a prototype neutron flux monitor with four collimated lines of sight² (the Neutron Camera (NC)) and a charged fusion products detector array³ were used for fast ion physics studies. The physics studies focussed on *i*) the interaction between fast ions with resonant and non-resonant MHD instabilities such as toroidal Alfvén eigen-

modes, fish-bones and long-lived modes and sawteeth^{4–6}, on *ii*) the effect of on- and off-axis NBI heating on the anomalous fast ion diffusion⁷ and on *iii*) the development of scenarios with good fast ion confinement⁸. The results of these studies contributed to the design of the plasma operating scenarios for MAST Upgrade⁹ (MAST-U) and to design of the NBI geometry for optimized current drive and fast ion confinement. MAST-U consists of a series of phased upgrades. For the purpose of neutron emission measurements, the phases are: “core scope” (the initial phase) characterized by two NBI systems with a total of 5 MW input power (one on-axis and one off-axis, 65 cm above the equatorial plane), “stage 1” in which an additional 2.5 MW off-axis NBI will be added and finally “stage 2” which will see the installation of another 2.5 MW on-axis NBI. In preparation for fast ion physics studies on MAST-U, several conceptual studies for an upgraded NC were carried out¹⁰ all with the goal to increase the spatial resolution. The NC had four Lines of Sight (LoS), two on-axis and two off-axis, all viewing the plasma in tangential (toroidal) direction with a spatial resolution of 20 cm. Neutron emissivity profiles were probed with higher spatial resolution by moving the NC in between pulses and by repeating similar plasma discharges. However, MHD instabilities are not exactly reproducible from discharge to discharge making the interpretation of the observations more complicated. This paper presents the solutions adopted for the Neutron Camera Upgrade (NCU) that will be installed on MAST-U, the design criteria on which it was based together with the results from the characterization of the neutron detectors.

^{a)}Contributed paper published as part of the Proceedings of the 22nd Topical Conference on High-Temperature Plasma Diagnostics, San Diego, California, April, 2018.

^{b)}Electronic mail: marco.cecconello@physics.uu.se

II. MAST-U SCENARIOS

Extensive predictive TRANSP¹¹/NUBEAM¹² simulations were carried out for MAST-U. Of particular relevance for the design of the NCU are the simulations for scenarios A, dedicated to stability and confinement studies, and for scenarios C and D dedicated to the study of the confinement of fast ions and the efficiency of different NBI current drive methods. Different levels of on-axis and off-axis NBIs heating and of anomalous fast ion diffusion resulted in neutron rates varying between 10^{14} and 10^{15} s^{-1} with a wide variation in the neutron emissivity $\varepsilon(R, Z)$ as shown in figure 1, from highly peaked profiles for an anomalous fast ion diffusion coefficient $D_a \lesssim 0.3 \text{ m}^2 \text{ s}^{-1}$ (simulation “K26”) to more flat profiles for $D_a = 5 \text{ m}^2 \text{ s}^{-1}$ (“L86”). These two plasma scenarios are characterized by 5 MW of NBI power, a plasma current of 1 MA, a density of $2 \times 10^{19} \text{ m}^{-3}$ and temperature in the range 1 to 2 keV.

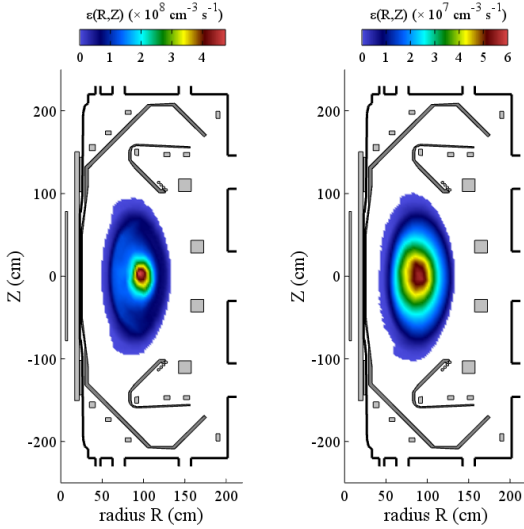


FIG. 1. Neutron emissivity $\varepsilon(R, Z)$ representative of the highest (K26, left panel) and lowest (L86, right panel) neutron yield according to TRANSP prediction for “core-scope” scenarios in MAST-U with low and high anomalous fast ion diffusivity (0.3 and $5 \text{ m}^2 \text{ s}^{-1}$ respectively). Poloidal magnetic field coils are shown in light grey, the first wall in dark grey.

III. DESIGN PRINCIPLES AND SOLUTIONS

The overall design criteria used for the final design of the NCU were: (1) a time resolution of 1 ms with a maximum of 10 % statistical uncertainty on the counts above threshold for each LoS, with a maximum zero-threshold count rate smaller than 1 MHz; (2) a spatial resolution along the major radius of 10 cm for a single plasma discharge; (3) an improved shield against γ -rays from thermal capture of neutron in the polyethylene shield; (4) an energy resolution better than 10 % for 2.5 MeV neutrons; (5) compatibility with the increased stray magnetic fields expected in MAST-U; (6) compatibility with port allocation engineering and interfacing constraints; (7) retaining

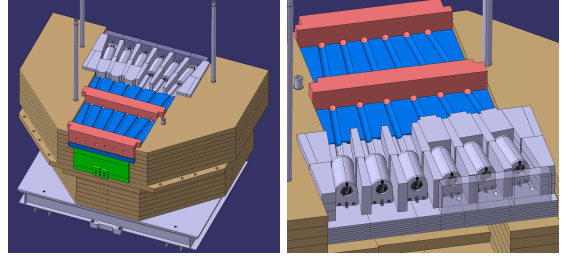


FIG. 2. Front and back views CAD models of NCU: collimators (blue), detectors and lead shielding (grey), HDPE shielding (light brown and green).

as many components as possible of the original prototype NC; (8) acquisition system located outside the MAST-U experimental hall (path length of signal cables between 30 and 40 m).

As a result of points (6,7), the NCU is now located further away from MAST-U centre and its overall outer dimensions and material of the neutron shield are the same as those of the NC. The implications of these constraints on the geometry of the lines of sight is discussed in section III A. Observation of the plasma is in the counter-clock wise direction only due to interfacing with other diagnostic systems. The detection system consists of EJ-301 liquid scintillators coupled to PM tubes and is described in section III B while the shielding is described in section III C.

A. Geometry of the lines of sight and collimators

The neutron emissivity $\varepsilon(R, Z)$ is converted into counts at the detector by taking into account the solid angle of each field of view¹³. The collimator’s length L and diameter D and the detector active layer’s thickness were adjusted to provide the required count rates. The number of lines of sight was limited to a maximum of six due to the constraint on the outer dimension of the neutron shield and to required spatial separation of each lines of sight (no overlapping collimators). Higher spatial resolution will be achieved by rotating the NCU around a pivot point in-between plasma discharges by re-using the NC supporting frame and rail. In contrast to the NC, where the pivot and the LoS focal points coincided, it has been necessary to separate the two in the NCU design: the pivot point is located at 2.9 m from MAST-U centre while the focal point is at 2.1 m. The axis through the pivot and focal points defines the axis of the NCU and corresponds to an impact parameter $p = 0.85 \text{ m}$: this is referred to as the reference position (rotation angle $\theta = 0^\circ$). The six collimators have all the same diameter $D = 3 \text{ cm}$ and length $L = 1.035 \text{ m}$ with an angular separation of 3° and are shown in figure 2. In the reference position, the impact parameter ranges from 0.6 to 1.1 m with a 10 cm separation. The LoS focal point coincides with the centre of the equatorial flange through which the plasma is observed. A circular area on the flange with a diameter of 28 cm diameter has been machined down to 4 mm thickness (see section III C). This area and the

size of the field of views' footprint limit the range of rotation around the pivot point to 8° s corresponding to $p \in [0.33, 1.23]$ m sufficient to measure the entire region of significant neutron emissivity. Rotation by $\theta = 1^\circ$ results in $\Delta p = 5$ cm: a spatial resolution of 5 cm can thus be achieved with the repetition of only two discharges.

B. Detection system

Six identical detectors have been designed for the NCU. The EJ-301 liquid scintillator active volume is a cylinder with a diameter of 3 cm and a thickness of 1.5 cm. MCNP simulations estimate the zero threshold efficiency to be $\approx 17\%$ for 2.5 MeV neutrons. The EJ-301 is coupled to a Hamamatsu R7761-70 PMT via an 11 mm thick optical window. A fiber optic is glued to the window and used to shine blue light onto the PMT from a LED source for monitoring the gain stability and linearity of the detector. A 30 m long optical fiber has been designed to connect the LED source to the detector and consists of an initial 0.5 m long fiber splitting into a bundle of six fibers, one for each detector. The intensity of the light output across the six different fibers is quite uniform with a maximum relative variation of approximately 6 %. Each detector is equipped with an embedded ^{22}Na γ -ray source for calibration purposes located near the active volume in an inset on the side wall of the casing. The source activity is 20 kBq, low enough not to perturb the measurements during plasma operation. The thickness of the aluminium casing on the detector side facing the plasma is 1 mm thick to reduce neutron scattering and attenuation. For the same reason, a circular region of the vacuum flange through which the NCU sees the plasma has been machined to a 4 mm thickness. The expected reduction of the direct neutron flux, estimated via MCNP, is approximately 0.87. Each of the 43 mm long PMTs is surrounded by a 1 mm thick μ -metal shield and the detector itself is placed inside two, 20 cm long, 5 mm thick soft iron cylindrical magnetic field shields so that their centres coincide. Simulation of the stray magnetic field inside the magnetic shield estimates a residual stray field of less than 0.3 mT for currents in the poloidal field coils at their maximum rating. The detector assembly, shown in figure 3, is designed so that the front face of the collimator is 5 cm further away from the back end of the collimator to reduce the contribution from in-scattered neutrons. A MCNP calculation indicated that the ratio between in-scattered and direct neutrons drops from 2.6 % to 1.1 % when the detector is at this location and that to reduce it below 0.5 % would require the detector to be placed 20 cm away. Given the spatial and weight constraints a 5 cm distance was considered a good compromise. The expected counts above threshold (11 % efficiency) for an integration time of 1 ms are shown in figure 4 for the neutron emissivities shown in figure 1 with the NCU in its reference position and with $\theta = 1^\circ$. Counts varies between 100 and 400 for “L86” and between 700 and 200 for “K26”. Compatibility with the expected higher count rates for “stage 1” and “stage 2” scenarios will be achieved by reducing the collimator’s

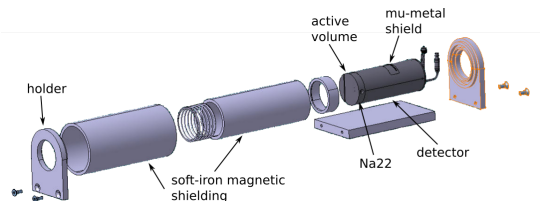


FIG. 3. CAD model exploded view of the NCU detector, the double magnetic shielding and the front and back holders.

diameter to 2 cm via the use of inserts which results in an expected reduction of the count-rate above threshold by a factor 5 (a doubling of the count rate for a ten-fold increase in the neutron rate). The acquisition system consists of the two double-channel digitizers used in the NC (Spectrum M3i.4121, 250 MSamples/s with 14-bit resolution and 256 MB on-board memory) to which a more recent version of the same digitizer has been added to maintain backward compatibility with the data acquisition and data analysis software.

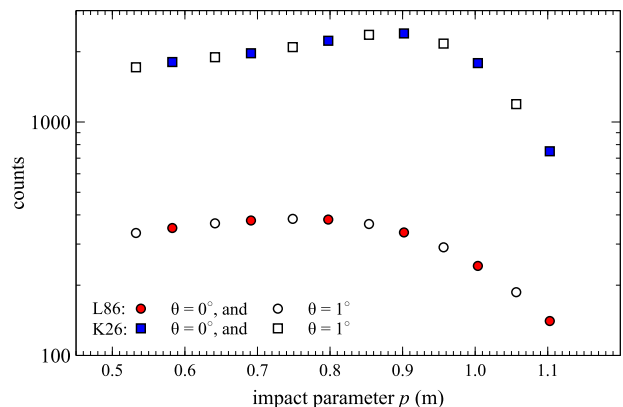


FIG. 4. Expected counts above threshold in the NCU detectors for 1 ms integration time and an efficiency of 11 % for the two scenarios shown in figure 1 when the NCU is in its reference position (solid circles) and when rotated by 1° (empty circles).

C. Collimation and shielding

Collimation and shielding against scattered neutrons are achieved by a massive High Density PolyEthylene (HDPE, with a density of 0.95 g/cm^3) shield surrounding the detector area. The overall outer dimensions are the same as those of the NC shield. The internal part of the HDPE shield has been redesigned to host the six collimators (the blue coloured parts in figure 2). Shielding against 2.2 MeV γ -rays from the thermal neutron capture reaction $\text{H}(n,\gamma)\text{D}$ is provided by slabs of lead of different thickness but a no point the thickness seen by the active volume is less than 10 cm. In particular, the last 20 cm of the collimation are realized by lead blocks rather than HDPE to reduce the high γ -ray count rates observed in the NC (which was comparable to the neutron rate). MCNP simulations indicate that with this

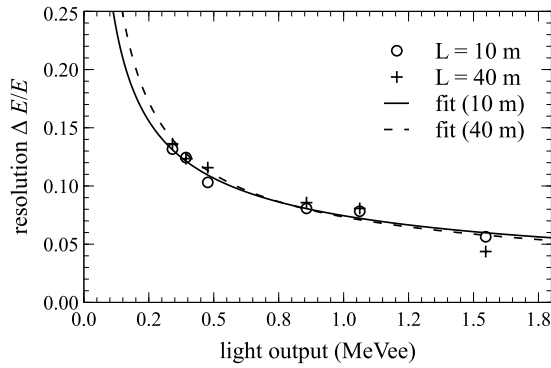


FIG. 5. Energy resolution measured with ^{22}Na , ^{137}Cs and ^{207}Bi γ -ray sources with short and long cables (open circles and crosses respectively) and fitted energy resolution functions (solid and dashed lines respectively). The energy resolution function parameters α , β and γ obtained by a least-squared fit of the experimental data are reported in the main text

design the total count rate above threshold is expected to be reduced from 1 MHz to 0.55 MHz of which only 50 kHz are from γ -rays. The reduced count rate will help in maintaining a good linearity of the PMT gain. The increased lead shielding in front of the detectors and of the volume in going from four to six detectors on the same plane resulted in the increase of the weight from about 4.5 to about 8 tons which has required the reinforcement of the wooden floor support structures on which part of the NCU load rests as well as a redesign of trolley with the addition of two front wheels to remove any loading on the pivot point. Detailed MCNP/ADVANTG calculations were carried out of the neutron field in the MAST area for the NC shield: the estimated neutron fluxes with energy in the range 1 eV - 2.45 MeV at the detector location are of the order of 10^{-13} per source particle per cm^2 , reduced by 7 orders of magnitude with respect to the incident neutron flux on the shield outer surface. In fact, no neutrons were detected in the NC with the collimator closed². The NCU detectors are located in within this region and therefore the present outer shielding is considered sufficient. Most of the scattered neutrons in the detectors' region will be instead generated by neutrons travelling along the collimator. The thermal (~ 1 eV) component of the neutron flux in this region is approximately 10^{-11} per source particle per cm^2 . On MAST-U the overall neutron flux is expected to increase by a factor 10 and although it is expected that the present shielding is sufficient, especially for the “core scope” scenario, detailed MCNP calculations will be carried out.

IV. DETECTOR CHARACTERIZATION

One of the NCU detector has been characterized with short (10 m) and long (40 m) RG58 co-axial signal cables with standard calibration γ -ray sources and with a ^{252}Cf neutron/ γ -ray source. The detector response function to ^{22}Na , ^{137}Cs and ^{207}Bi γ -rays was measured in the laboratory. The energy resolution at each Compton

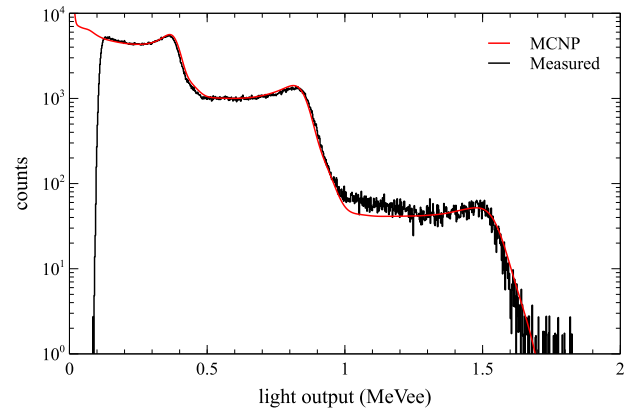


FIG. 6. Comparison between the measured (black) and MCNP simulated (red) light output pulse height spectrum for ^{207}Bi γ -ray source.

edge energy is shown in figure 5 together with the fitted energy resolution function. The resolution function parameters obtained from the fit are: $\alpha = 0.011$, $\beta = 0.072 \text{ MeV}^{-1/2}$ and $\gamma = 0.014 \text{ MeV}$ and $\alpha = 0.0$, $\beta = 0.069 \text{ MeV}^{-1/2}$ and $\gamma = 0.026 \text{ MeV}$ for short and long cables respectively. As can be seen the length of the co-axial cables does not affect the energy resolution function particularly in the region of interest around 0.8 MeVee which corresponds to the light output deposited by a recoil proton after it has undergone an head-on collision with a direct neutron of 2.5 MeV energy. In particular, the energy resolution is better than a factor of two for all energies of interest compared with the NC detectors² thanks to the more compact cylindrical design of the scintillator with improved light collection. The measured pulse height spectrum for each γ -ray source, background subtracted, was then compared with MCNP simulations in which the measured energy resolution function was converted into the FT/GEB tally modifier used to introduce a Gaussian energy broadening in the F8 energy deposition tally. Good agreement between measurements and simulations was observed for all γ -ray sources and an example is shown in figure 6.

The neutron/ γ -rays Pulse Shape Discrimination (PSD) is shown in figure 7 where the distribution of the discrimination parameter $D_{n,\gamma} = 1 - Q_F/Q_T$ is shown against the total light output. Q_F and Q_T are the fast and total charge calculated for each individual pulse in the time intervals indicated in figure 8. As can be seen in figure 7, the detector maintain a good PSD capability also in the case of long signal cables. The long signal cables reduce the amplitude of the pulses in input to the ADC and act as low-pass filter as clearly seen by comparing panels (a) and (b) of 8. The Figure of Merit (FOM) parameter F is shown in figure 9 as a function of the total light output for short and long cables corresponding to the data shown in figure 7. Panel (a) of figure 9 shows the figure of merit F of the PSD defined as $F = |P_n - P_\gamma|/(FWHM_n + FWHM_\gamma)$. $FWHM_{n,\gamma}$ is the full-width at half-maximum and $P_{n,\gamma}$ the centroid of the two Gaussian distribution fitting the histogram of $D_{n,\gamma}$ from a narrow light output interval as shown in panel (b) of figure 9. As can be seen, although

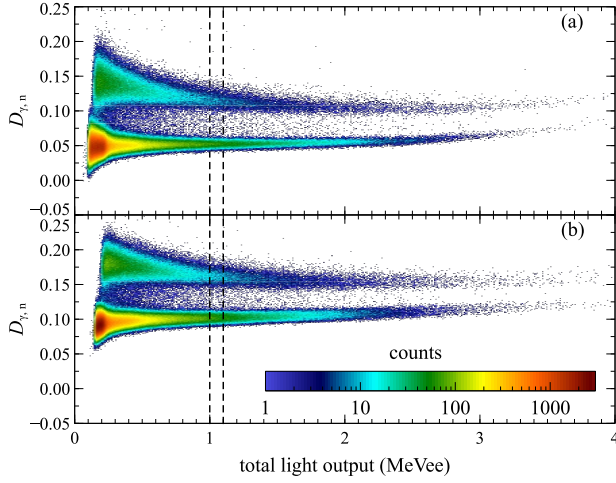


FIG. 7. Distribution of neutron and γ -ray pulses from a ^{252}Cf source as a function of the total light output and of the discrimination parameter $D_{\gamma,n}$ for short (a) and long (b) cables. The vertical dashed lines indicates the width of the interval used for the calculation of the figure of merit shown in figure 9.

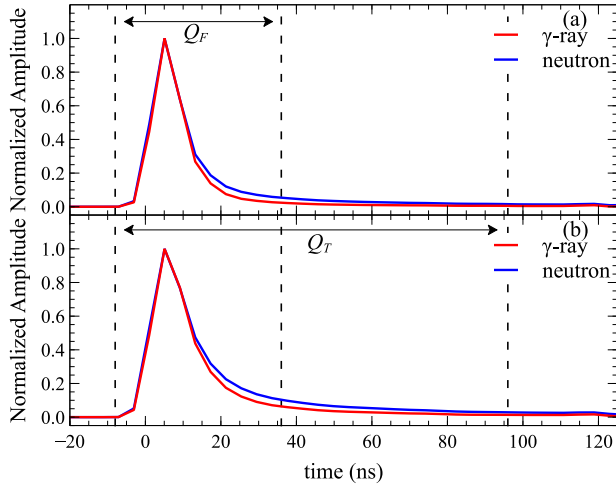


FIG. 8. Normalized neutron and γ -ray pulses from a ^{252}Cf source measured with short (panel(a)) and long (panel(b)) coaxial cables connecting the detector to the ADC. The curves are obtained from averaging over multiple pulses for a light output in the range $[0.95, 1.05]$ MeVee.

the FOM decreases at high light output yields for the case with long cables, the FOM is still quite good given the limited sampling frequency¹⁴ of the present ADC system.

V. CONCLUSIONS

The proposed NCU is expected to meet all its target measurement requirements for contributing to the fast ion physics studies on MAST Upgrade. In particular, thanks to the improved energy resolution of the detector, it is expected that a better measurement of the neutron

energy spectral components would be possible. The

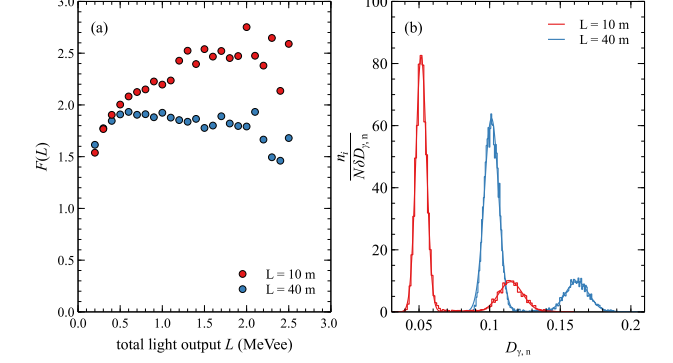


FIG. 9. Figure of merit (panel (a)) as a function of the energy deposited by recoil electrons and protons in the EJ-301 exposed to a ^{252}Cf source for 10 and 40 m long cables connecting the detector to the ADC. The normalized probability density function and fit for $L = 1$ MeVee is shown in panel (b) where n_i is the number of counts per bins, N is the total number of counts in the selected region and $\delta D_{\gamma,n}$ is the bin width.

NCU is expected to begin commissioning during the fall of 2018 and first plasma measurements are planned for the beginning of 2019.

ACKNOWLEDGMENTS

This work was funded by the Swedish Research Council, the RCUK Energy Programme under grant EP/P012450/1, the European Unions Horizon 2020 research and innovation programme under grant agreement number 633053 and the U.S. Department of Energy Contract Numbers DESC0001157 and DEAC0209CH11466. The views and opinions expressed herein do not necessarily reflect those of the European Commission.

- ¹M. Cox *et al.*, Fusion Eng. Des. **46**, 397 (1991).
- ²M. Cecconello *et al.*, Nucl. Instrum. Meth. **72**, 753 (2014).
- ³R. V. Perez *et al.*, Review of Scientific Instruments **85**, 11D701 (2014).
- ⁴M. Cecconello *et al.*, Plasma Physics and Controlled Fusion **57**, 014006 (2015).
- ⁵O. M. Jones *et al.*, Plasma Physics and Controlled Fusion **57**, 125009 (2015).
- ⁶M. Cecconello and A. Sperduti, Plasma Physics and Controlled Fusion **60**, 055008 (2018).
- ⁷M. Turnyanskiy *et al.*, Nuclear Fusion. **53** (2013).
- ⁸D. Keeling *et al.*, Nuclear Fusion **55**, 013021 (2015).
- ⁹A. W. Morris, IEEE Trans. Plasma. Sci. **40**, 682 (2012).
- ¹⁰M. Weiszflog, S. Sangaroon, M. Cecconello, S. Conroy, G. Ericsson, I. Klimek, D. Keeling, R. Martin, and M. Turnyanskiy, Review of Scientific Instruments **85**, 11E121.
- ¹¹J. Hawryluk, R. *An Empirical Approach to Tokamak Transport*, edited by B. Coppi, Vol. 1 (CEC, Brussels, 1980) p. 19.
- ¹²A. Pankin, D. McCune, A. Robert, G. Bateman, and A. Kritiz, Comput. Phys. Commun **159**, 157 (2004).
- ¹³I. Klimek *et al.*, Nuclear Fusion **55**, 023003 (2015).
- ¹⁴C. Hellesen, M. Skiba, G. Ericsson, E. A. Sundén, F. Binda, S. Conroy, J. Eriksson, and M. Weiszflog, Nuclear Instruments and Methods in Physics Research Section A: Accelerators, Spectrometers, Detectors and Associated Equipment **720**, 135 (2013).